frontiers | Frontiers in Earth Science

ORIGINAL RESEARCH
published: 12 April 2022
doi: 10.3389/feart.2022.879654

Rhyolitic Ash Promoting Organic Matter Enrichment in a Shallow Carbonate Platform: A Case Study of the Maokou Formation in Eastern Sichuan Basin

Qingqiang Meng[1,2,3]*, *Qian Pang*[4], *Guang Hu*[4]*, *Zhijun Jin*[1,3,5], *Donhya Zhu*[1,3], *Jiayi Liu*[1,3] and *Chuanwen Zhang*[6]

[1]State Key Laboratory of Enrichment Mechanism and Effect Development of Shale Oil and Gas, Beijing, China, [2]State Key Laboratory of Organic Geochemistry, Guangzhou Institute of Geochemistry, Guangzhou, China, [3]Petroleum Exploration and Product Research Institute, Beijing, China, [4]School of Geoscience and Technology, Southwest Petroleum University, Chengdu, China, [5]Institute of Energy, Peking University, Beijing, China, [6]School of Energy, Chinese University of Geosciences (Beijing), Beijing, China

OPEN ACCESS

Edited by:
Chen Zhang,
Chengdu University of Technology, China

Reviewed by:
Xiaoqiang Li,
Texas Tech University, United States
Fujie Jiang,
China University of Petroleum, Beijing, China

***Correspondence:**
Qingqiang Meng
mengqq.syky@sinopec.com
Guang Hu
guanghu1198119@163.com

Specialty section:
This article was submitted to Structural Geology and Tectonics, a section of the journal Frontiers in Earth Science

Received: 20 February 2022
Accepted: 07 March 2022
Published: 12 April 2022

Citation:
Meng Q, Pang Q, Hu G, Jin Z, Zhu D, Liu J and Zhang C (2022) Rhyolitic Ash Promoting Organic Matter Enrichment in a Shallow Carbonate Platform: A Case Study of the Maokou Formation in Eastern Sichuan Basin. Front. Earth Sci. 10:879654. doi: 10.3389/feart.2022.879654

Volcanic ash improves the amount of nutritive elements in the lake and ocean, but it is not fully understood how volcanic ash influences the total organic matter content (TOC) and bio-precursor, and the scope. A volcanic layer, measuring 5 cm in thickness, was examined using electron microscopy scanning, TOC/TS, rock pyrolytic, and inorganic geochemical analyses. The study shows that the TOC content in the overlying shales increases by 18 wt.% on average, and the vertical scope of influence on shales is twice as thick as the volcanic layer. Organic matter enrichment is attributed to the fact that the volcanic layer provides nutritive elements and meanwhile changes the oxidation-reduction condition. Large variations of hydrogen index (HI) and oxygen index (OI) in the lower and upper parts of the volcanic layer is related to terrestrial organic matter vanishing, due to volcanic eruption and subsequently more terrigenous organic matter migrating into the ocean. Little change of the bio-precursor in the overlying and underlying shales may be related to the fast restoration within the ocean and land ecosystems after a volcanic eruption. The decrease in terrigenous sediments indicated by Rb/Sr, Zr/Y, and ∑REE after a volcanic eruption indirectly reflects fast restoration of terrestrial vegetation boom. This study could decipher the influence of volcanic ash on the qualities of the source rock, which can provide a better understanding on discovering more economically petroleum reservoirs in igneous rocks.

Keywords: volcanic ash, organic matter, productivity, bio-precursor, hydrocarbon generation, Maokou formation, Sichuan Baisn

1 INTRODUCTION

Volcanic ash is the eruptive magmas sediments composed of vitric fragments, rock fragments, and crystal fragments, with a diameter smaller than 2 mm, that may float thousands of kilometers away (White and Houghton, 2006). Recent studies have shown that volcanic ash may cause an algae bloom and increase chlorophyll-a content in seawater. This phenomenon is widely observed in marine and

lake after recent volcanic eruptions (Uematsu et al., 2004; Duggen et al., 2010; Hoffmann et al., 2012). Therefore, it is of great significance to demonstrate the impaction of volcanism on the change of sedimentary environment and the formation of source rocks.

Preceding studies showed the important effect of volcanic ash on organic matter enrichment in source rocks (Guoheng Liu et al., 2019), e.g., the Eagle Ford and Marcellus Shales in the US (Zeng et al., 2018), the seventh member in the Yanchang Formation, the Ordos Basin, China (Qing Li et al., 2020; Zhang et al., 2020), the Lucaogou Formation in the Junggar Basin (Jingya Zhang et al., 2019; Quanyou Liu et al., 2019; Shaomin Zhang et al., 2019), the Longmaxi Formation in the Sichuan Basin (Yan et al., 2018), and oil shales in the Bazhenov Formation, Russia (Liang et al., 2021).

As for the relation between volcanic ash and black shales in geologic history, volcanic ash may increase total organic carbon content (Guoheng Liu et al., 2019; Jingya Zhang et al., 2019; Shaomin Zhang et al., 2019; Li Li et al., 2020; Qing Li et al., 2020; Si et al., 2020; Zhang et al., 2020), alter organic matter type (Li Li et al., 2020; Si et al., 2020), change climate (Tao et al., 2020), and affect water oxidation-reduction (Liu et al., 2007). However, ash-bearing source rocks tend to be related to anoxic environments, marine transgressions, and upwelling currents (Zhao et al., 2020), which will similarly enrich the organic matter content. Therefore, it is difficult to separate all these factors and evaluate the effect of volcanic ash on source rocks. The neritic carbonate platform in the Maokou Formation is a good candidate to study, in view of its non-anoxic environment and non-upwelling effect (Gao et al., 2020).

To assess the influence of volcanic ash on organic matter, the TOC content, hydrogen index (HI), and oxygen index (OI), of the shales above and below the volcanic layer are usually used for comparison to establish the effect of volcanic ash on organic matter content and type (Zhao et al., 2020). However, these investigations seldom dealt with the duration of organic matter deposition, which may be promoted/inhibited by volcanic ash due to the lack of organic geochemical indexes. The ash thickness could be affected by the intensity of influence and mechanism. According to the study of recent volcanic eruptions, volcanic ash will release salts, which contain P, Fe, and Mn, altering organism type and content (Hoffmann et al., 2012) when the ash flows into water. On the other hand, volcanic ash will consume mass oxygen, changing sediments and water oxidation-reduction (Haeckel et al., 2001; Hembury et al., 2012; Longman et al., 2019, 2020). Above variations will be imprinted by inorganic elements in sediments. This means that it is possible to more deeply understand the effect of volcanic ash on organic matter enrichment through detailed high-precision sampling to verify the change in elements above and below the volcanic layer.

This study involves the Maokou Formation of Middle Permain containing volcanic ash in the Lengshuixi tunnel section in the Sichuan Basin, Shizhu County, China. The study focuses on 1) Terrestrial environmental responses before and after a volcanic eruption, 2) Perturbation of source organisms by a volcanic eruption, and 3) TOC variation before and after a volcanic eruption and the mechanism of volcanic ash effect on organic matter enrichment. Resulting evaluations are based on the analysis of volcanic ash type, origin, shale geochemistry, and organic petrology using organic geochemical, inorganic geochemical, and mineralogical techniques.

2 GEOLOGIC SETTING

The Paleo-Tethys Ocean became more active during Permian, which resulted in the fault subsidence of the southern Qinling, and the origin of a rifted continental margin extending in a northwest direction in western Sichuan and western Yunnan (Ji et al., 1997). At the end of the Permian Period, the Emei basalts as covered with 250,000 km^2. The lava sheet was mainly composed of basaltic and andesitic volcanic rocks in the lower part and felsic volcanic rocks in the upper part (Xu et al., 2001; Xiao et al., 2004). Felsic volcanic rocks (rhyolites and trachytes) have been reported to locally occur in Binchuan and Panzhihua (Shellnutt and Jahn, 2010; Xu et al., 2010).

During the Middle Permian Epoch, in the Maokou Formation of the upper Yangtze region, deposits of a carbonate platform environment were formed and were composed of bioclastic limestones, micrite, and some shales (**Figure 1A**). The study samples were acquired from a lithologic association of 60 cm thick, consisting of marls, shales, and volcanic tuffs. These samples were obtained from an outcrop section in the Maokou Formation of Middle Permain close to the Lengshuixi tunnel in Shizhu County, Chongqing. In this outcrop section, 5 cm of volcanic ash is sandwiched between two 25 cm layers of greyish black shale, apart from which there are grey marls. A significant amount of moss was growing on the volcanic ash, while only some scattered moss grew on the overlying and underlying black shales (**Figure 1B**).

3 MATERIALS AND METHODOLOGY

The weathering surface was removed first, followed by sampling. 25 samples were acquired from the 60 cm thick lithologic association in the Maokou Formation, among which 14 were from underlying formations of volcanic ash, four from volcanic ash, and seven from overlying formations of volcanic ash. As for volcanic ash, overlying shales, and underlying shales, each layer was acquired with one moss sample.

Volcanic ash samples were observed using a field emission scanning electron microscope (SEM). The samples were first prepared in 1 cm^3 cubes, and then the natural fracture surfaces were sprayed with gold using a coater. Mineral geometry and structure were observed in a high vacuum condition of the scanning electron microscope and the elements were checked using energy spectra. The accelerating voltage was set at 15 kV. The experiments were performed at the School of Geoscience and Technology, Southwest Petroleum University, China.

TOC/TS testing was carried out using an organic carbon/sulphur analyzer (CS230SH) for all 26 samples. Before conducting the experiments, all the samples were cleaned using hydrochloric acid to eliminate inorganic carbon and

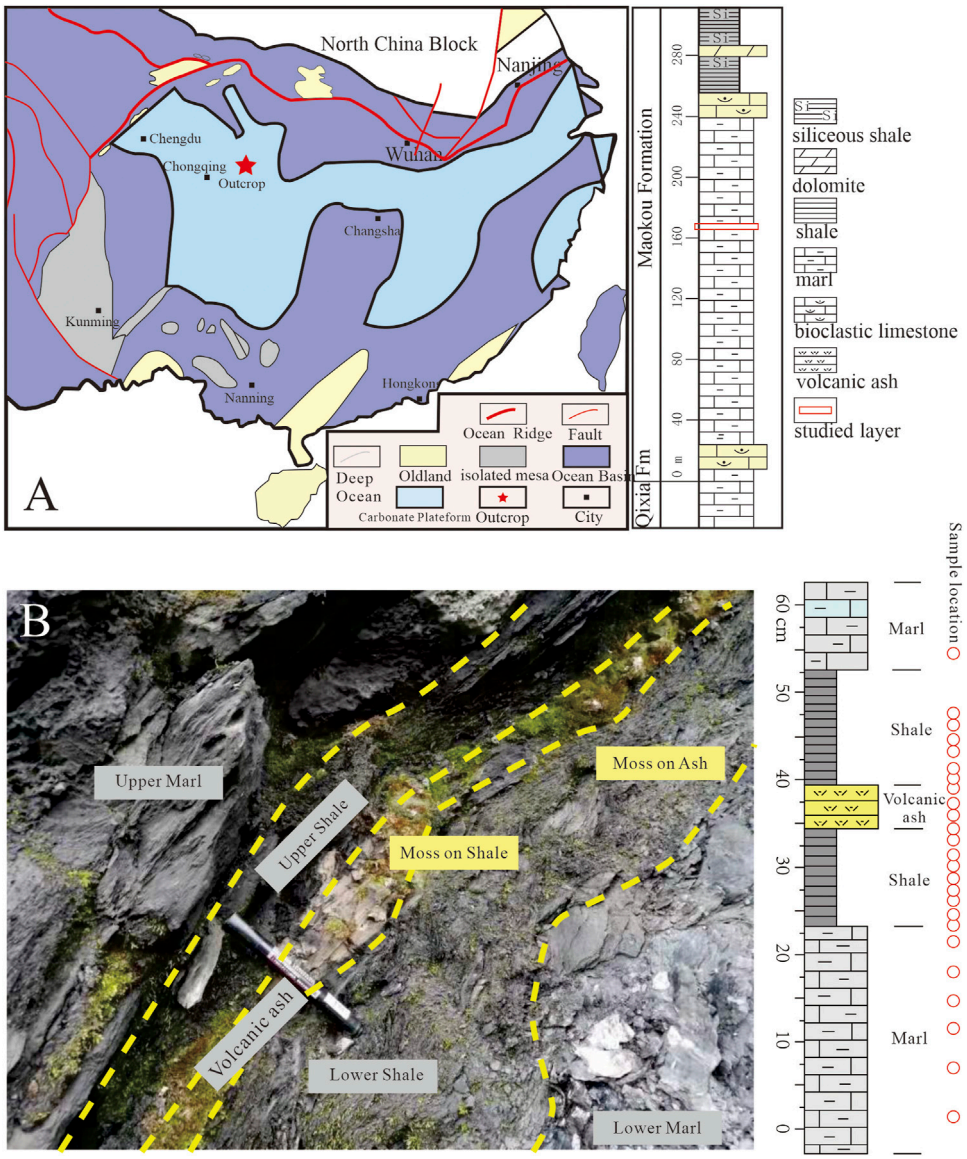

FIGURE 1 | Outcrop location **(A)** and the micro section composition **(B)** [A modified from Luo (2009)].

ions on the surface, e.g., Na, Cl, and Ca, and finally dried in an oven. These experiments were performed at the State Key Laboratory of Oil and Gas Reservoir Geology and Exploitation, China.

Pyrolytic experiments were made by Delsi Rock-Eval RE II. As the temperature increased, liquid hydrocarbons (S_1) were released first, followed by cracked hydrocarbons (S_2) as well as carbon dioxide and carbon monoxide (S_3). HI = (100 × S_2)/TOC; OI = (100 × S_3)/TOC.

The 25 samples were carried out for major elements, trace elements, and rare Earth elements (REE). Powdered samples, of 200 mesh, were dissolved using aqua regia. Nitric acid-hydrofluoric acid digestion ICP-MS was employed, and a PlasmaQuant MS Elite ICP-MS analyzer was used during this procedure. International reference samples OU-6, AMH-1, and GBPG-1 were used for quality control with an analytical error of less than 10%. Refer to Ling et al. (2021) for detailed workflow. For all the samples, the analytical error was estimated to be less than 5%. The experiments of major elements, trace elements, and REEs were made in State Key Laboratory of Ore Deposit Geochemistry-Institute of Geochemistry, Chinese Academy of Sciences.

With respect to ash analysis, the moss samples were cleaned using absolute ethyl alcohol, a minimum of 10 times, or until the dust and shale powder on the surface were eliminated. The samples were dried at normal temperature and then ground to an 80 mesh size. Each sample of 0.5 g was weighed and put into a polytetrafluoroethylene beaker for aqua fortis digestion. Element detection was made using the ME-VEG41gt method. The experiments were performed in ALS Minerals, Guangzhou, China.

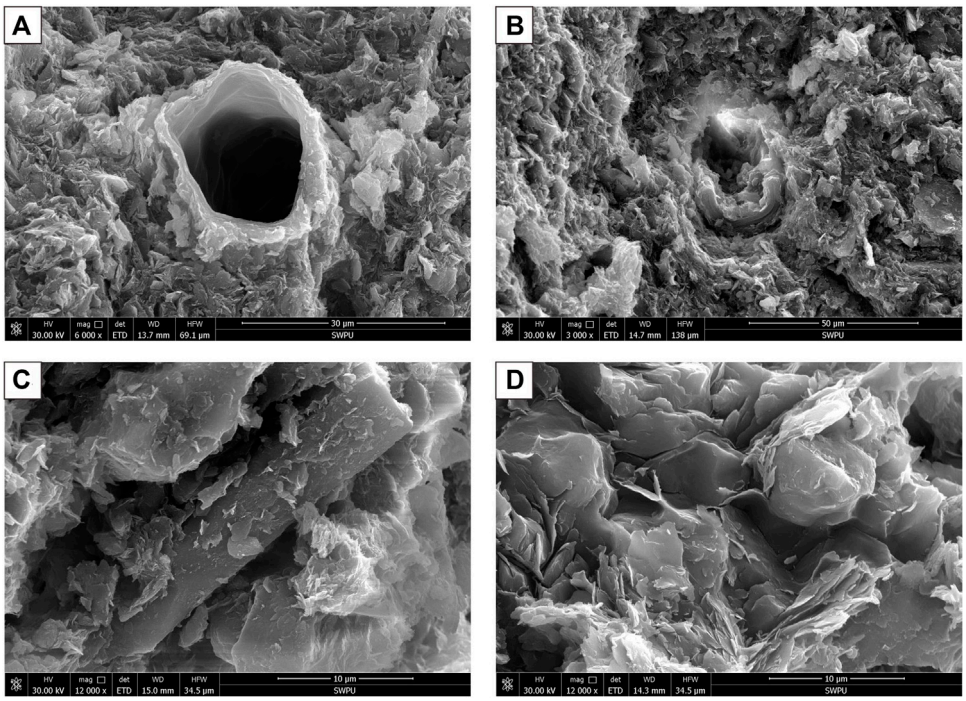

FIGURE 2 | SEM photos of quartzes in volcanic ash. **(A–C)**: hairline-like hollow quartzes. **(D)**: Aggregative quartzes.

4 RESULTS

4.1 Volcanic Ash Minerals

Clay and quartzes were the major minerals detected. The content of clay minerals, which may be the product of volcanic debris alteration, was as high as 90%. Quartzes in volcanic ash turn up in two forms. One is a hairline-like hollow tube known as Pele's hair, with an outer diameter of 24 μm, tube thickness of 1.46 μm, and length of 29.23 μm (**Figures 2A–C**). EDS energy spectra showed essential constituents of Si and O as well as some Fe, Ca, Al, Mg, and Zr (**Figures 2A,C**). The other is microcrystalline quartz-like aggregate with a particle diameter of 5.33–8.93 μm, major elements of Si and O, and some Mg and Zr (**Figure 2D**).

4.2 Organic Matter Content, TS, and Rock Pyrolysis

The section being examined included five layers; volcanic ash, overlying and underlying shales, and upper and lower mud shales (**Figure 1B**).

The overlying shale layer exhibits the highest TOC content at 0.856–1.140 wt.%, with an average of 1.056 wt.%. This is followed by the underlying shale layer with a TOC content of 0.827–0.948 wt.% and an average of 0.892 wt.%. The TOC content ranges from 0.283 wt.% to 0.769 wt.%, with an average of 0.506 wt.% in the volcanic ash layer, which are smaller than those in the overlying and underlying shale layers. The TOC content ranges from 0.240 wt.% to 0.793 wt.% with an average of 0.524 wt.% in the upper and lower marl layers.

The TS content was 0.095, 0.017, and 0.068% in the underlying shales, volcanic ash, and overlying shales, respectively. The value first decreases and then increases from the lower layer to the upper layer. (**Figure 3A**).

S_1, S_2, S_3, HI, and OI are shown in **Figure 4**. HI and OI do not vary greatly in the overlying and underlying shales, but they are obviously different in volcanic ash-I and volcanic ash-II. OI is higher in the volcanic ash-I than in the volcanic ash-II, whereas HI is lower in the volcanic ash-I than in the volcanic ash-II (**Figure 3A**).

4.3 Inorganic Elements

4.3.1 Major Elements

Ca content ranges from 10.70 to 22.30% in the marl layers, which is remarkably higher than in the shale layers, from 0.31 to 0.54% and volcanic ash layer from 0.45 to 0.55% (**Table 1**, **Table 2**; **Figure 3B**). Both shale layers show similar Ca and Mg contents, but Al, K, and Ti contents in the lower shale layer are higher than in the upper shale layer (**Table 2**; **Figure 3B**). Al, K, and Ti contents slightly increase in the lower shale layer and slightly decrease in the upper shale layer (**Figure 3B**).

In the moss sample from the volcanic ash layer, the Ca, Mg, K, Fe, P, and Mn contents are higher than in the samples from the shale layers, except for the S content. (**Figure 4**).

4.3.2 Trace Elements

Mo_{EF}, U_{EF}, and V_{EF} contents were generally less in the lower shale layer than in the upper shale layer (**Table 2**; **Figure 3B**). Fe and P contents were higher in the shale layers and volcanic ash layer than in the marl layers, but lower shales showed slightly higher Fe and P contents than upper shales (**Table 2**; **Figure 3B**). Cu/Al and Zn/Al were predominantly less abundant in lower shales than in upper shales (**Table 2**; **Figure 3B**).

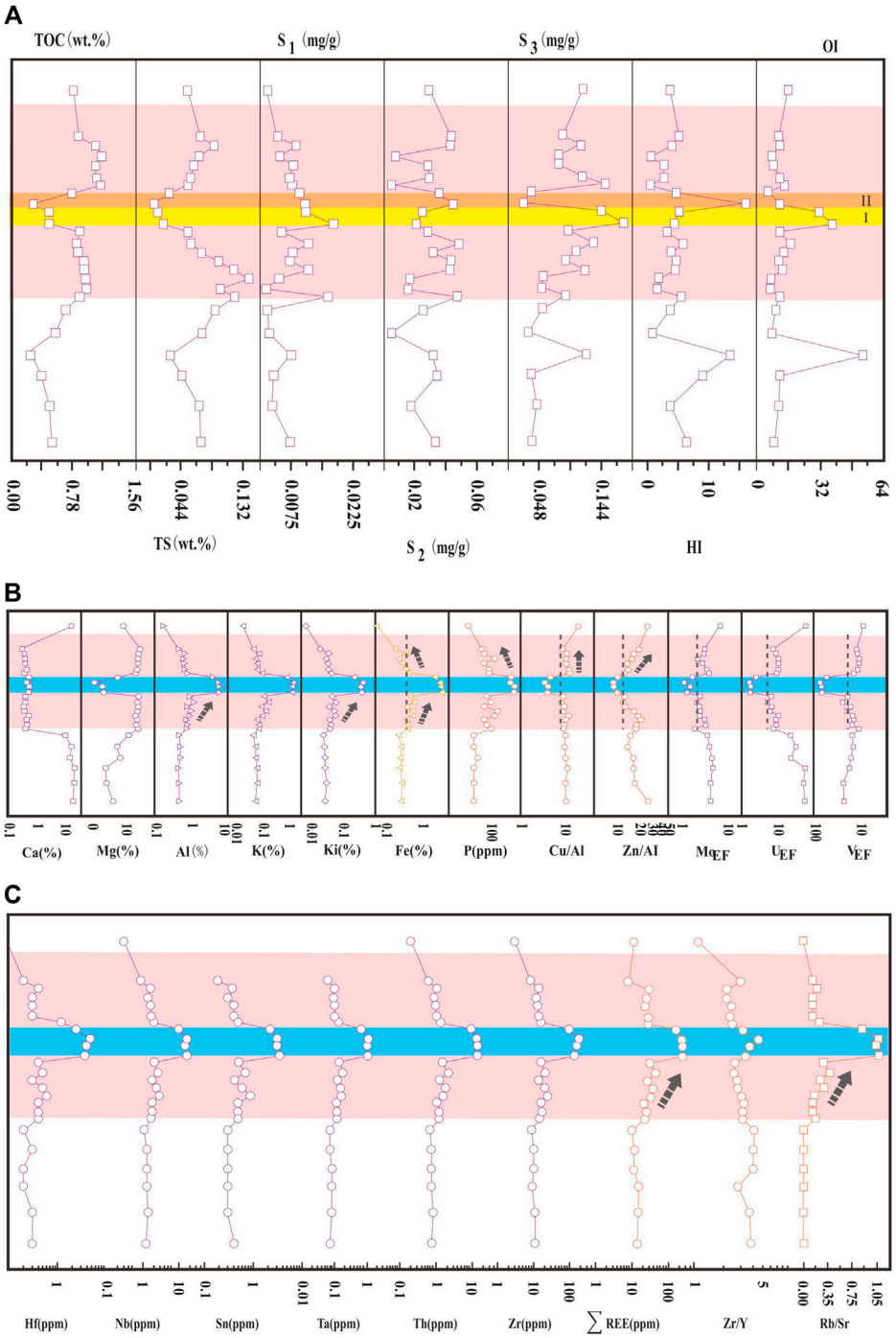

FIGURE 3 | Organic and inorganic geochemistry characters for different part of the micro section. **(A)**: Vertical distributions of TOC, TS, S_1, S_2, S_3, HI, and OI in the volcanic ash layer and upper and lower layers; **(B)**: Vertical distributions of major elements and other elements; **(C)**: Contents of immobile elements and vertical distributions of Zr/Y and Rb/Sr the lowest plain represents Lower Marl, the Lower pink means Lower shale and the blue belt for volcanic ash. The upper pink is for Upper shale and the plain part in the top is for Upper Marl in **Figure 1B**.

The contents of immobile elements, e.g., Hf, Nb, Sn, Ta, Th, and Zr, and ∑REE slightly increased from the deepest level in lower shales and slightly decreased from the lowest level in upper shales (**Figure 3C**). Zr/Y was more plentiful in lower shales than in upper shales. Rb/Sr increases upward in lower shales and basically remains unchanged in upper shales with decreased value (**Figure 3C**).

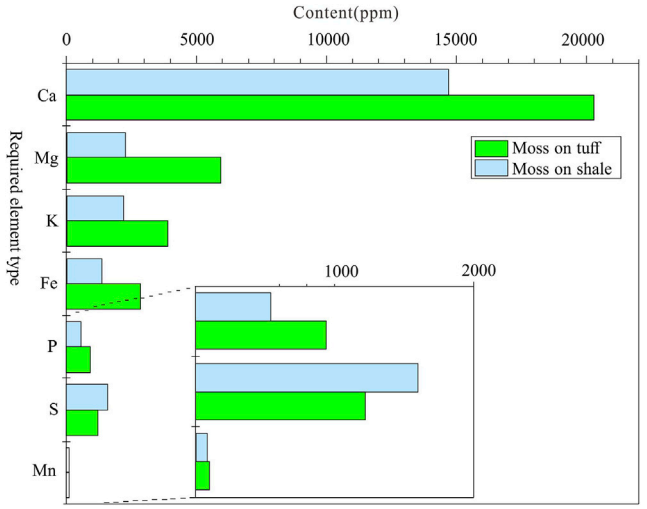

FIGURE 4 | Comparison of essential element content in the moss samples from the tuff layer and shale layers.

After mantle normalization of incompatible elements in volcanic ash, the spider diagram shows enriched large ion lithophile (LIL) elements (Cs, Rb, K, Ba, Sr, and Eu) and depleted high field strength (HFS) elements (**Figure 5**). Some elements (Ba, Nb, Ta, Sr, Zr, and Ti) are notably depleted (**Figure 5**).

4.3.3 REEs

Sedimentary rock and volcanic ash samples were normalized separately using post-Archean Australian shales and chondrites. As for sedimentary rocks, two marl layers showed a flat REE pattern (**Figure 6A**), which is similar to that of the marls in the Permian Maokou Formation (Su et al., 2020). Two shale layers showed a REE pattern of depleted light REEs, negative Ce/Ce* anomaly, and positive Y anomaly. The Ce/Ce*, an anomaly in the lower shales, was measured at 0.49–0.90, with an average of 0.70 at $n = 8$. This was higher than the upper shales at 0.42–0.50, with an average of 0.47 at $n = 6$. A La_N/Sm_N value of 0.74–1.09, with an average of 0.89 at $n = 8$, in the lower shales, was less than in the upper shales at 0.98–1.46, with the average of 1.09 at $n = 6$. This indicates more enriched REEs in the lower shales than in the upper shales (**Figures 6B,C**).

As for the volcanic ash REE pattern, a La_N/Yb_N value of 7.23–8.85, indicates more enriched light REEs (**Table 3**, **Table 4**). The Eu/Eu* value of 0.58–0.62, indicates a notable negative Eu/Eu* anomaly (**Table 4**; **Figure 6D**).

5 DISCUSSIONS

5.1 Volcanic Ash Origin and Type

SEM observation show the hollow quartz known as Pele's hair (**Figure 2**), is a typical kind of highly elongated volcanic debris (Duffield et al., 1977; Cannata et al., 2019). This denotes an intermediate-acidic magma eruption. The chondrite-normalized

TABLE 1 | TOC, TS, S_1, S_2, S_3, HI, and OI in the volcanic ash layer and upper and lower layers in the Lengshuixi section of the Maokou Formation.

Thickness (cm)	Lithology	TOC (wt%)	TS (%)	S_1 (mg HC/g)	S_2 (mg HC/g)	S_3 (mg HC/g)	HI	OI
1.9	1[a]	0.517	0.073	0.007	0.033	0.045	6.43	8.75
7.4	1	0.484	0.070	0.003	0.018	0.053	3.80	10.86
12.0	1	0.387	0.046	0.003	0.035	0.044	8.94	11.49
15.1	1	0.24	0.029	0.007	0.032	0.128	13.31	53.45
18.5	1	0.559	0.075	0.002	0.005	0.040	0.94	7.16
22.0	1	0.686	0.093	0.001	0.026	0.062	3.77	9.02
24.0	2	0.867	0.120	0.016	0.047	0.097	5.45	11.19
25.2	2	0.948	0.100	0.001	0.016	0.061	1.70	6.38
26.8	2	0.942	0.140	0.004	0.018	0.063	1.87	6.67
28.0	2	0.922	0.110	0.012	0.042	0.121	4.52	13.11
29.4	2	0.921	0.098	0.007	0.044	0.097	4.73	10.55
30.8	2	0.838	0.074	0.007	0.032	0.113	3.79	13.43
32.1	2	0.827	0.059	0.011	0.048	0.139	5.83	16.83
33.9	2	0.868	0.055	0.005	0.029	0.101	3.31	11.61
35.1	3	0.487	0.020	0.017	0.021	0.185	4.40	38.08
36.9	3	0.484	0.012	0.011	0.025	0.152	5.14	31.34
38.1	3	0.283	0.007	0.010	0.045	0.033	15.73	11.64
39.8	3	0.769	0.028	0.009	0.036	0.045	4.67	5.80
41.0	2	1.13	0.055	0.007	0.006	0.158	0.50	13.97
42.1	2	1.08	0.058	0.007	0.029	0.122	2.73	11.32
44.0	2	1.06	0.063	0.008	0.029	0.086	2.69	8.15
45.4	2	1.14	0.070	0.004	0.008	0.087	0.71	7.63
47.0	2	1.07	0.091	0.008	0.043	0.120	3.99	11.23
48.4	2	0.856	0.072	0.004	0.043	0.093	5.06	10.86
55.4	1	0.793	0.054	0.001	0.029	0.123	3.71	15.54

[a]*Lithology type:1 represents Grey marlstone; 2 represents Black Shale, 3 represents Volcanic ash, the same in blow tables.*

TABLE 2 | Contents and ratios of representative elements in the five layers in the Lengshuixi section.

Thickness (cm)	Lithology	Al (%)	Ca (%)	Mg (%)	K (%)	Ti (%)	Fe (%)	*p* (ppm)	Cu/Al	Zn/Al	Mo_{EF}	U_{EF}	V_{EF}
1.9	1	0.50	20.30	6.38	0.06	0.028	0.28	40	10.80	27.13	4.37	56.57	4.49
7.4	1	0.49	21.50	5.06	0.07	0.031	0.30	40	10.61	17.66	4.35	50.73	4.27
12.0	1	0.46	22.30	4.89	0.07	0.028	0.26	40	11.96	17.21	4.87	57.14	5.85
15.1	1	0.54	15.40	8.34	0.06	0.028	0.27	50	10.56	17.05	4.64	23.28	6.37
18.5	1	0.52	17.80	7.50	0.06	0.027	0.28	40	10.19	14.20	4.10	31.87	7.05
22.0	1	0.49	10.70	11.40	0.05	0.025	0.24	40	10.61	15.61	3.70	22.74	6.87
24.0	2	0.84	0.41	16.30	0.08	0.040	0.42	100	9.64	18.51	1.97	7.82	9.43
25.2	2	0.87	0.47	15.15	0.08	0.043	0.43	80	10.00	18.71	3.37	9.20	6.79
26.8	2	0.82	0.45	15.65	0.07	0.040	0.40	70	10.85	21.61	3.25	9.06	7.29
28.0	2	1.00	0.54	14.70	0.11	0.058	0.59	120	12.60	20.13	2.51	10.57	6.95
29.4	2	1.11	0.37	16.00	0.15	0.055	0.57	140	9.46	17.25	2.59	6.18	5.32
30.8	2	0.86	0.36	16.30	0.10	0.039	0.40	70	9.88	13.22	2.48	6.98	6.17
32.1	2	1.36	0.41	15.85	0.19	0.061	0.64	100	8.38	12.45	2.24	5.25	4.12
33.9	2	1.01	0.40	16.55	0.13	0.047	0.49	80	9.41	12.91	2.53	6.79	5.40
35.1	3	7.54	0.52	4.57	1.48	0.399	3.58	340	4.03	10.36	1.34	1.78	1.47
36.9	3	7.23	0.55	4.37	1.48	0.383	3.38	350	4.19	9.11	1.56	1.86	1.43
38.1	3	7.00	0.45	3.21	1.58	0.433	3.17	280	3.50	9.13	1.15	1.71	1.35
39.8	3	4.93	0.54	7.68	0.92	0.241	2.37	290	4.75	10.39	1.75	2.61	1.88
41.0	2	0.88	0.38	15.05	0.11	0.045	0.44	90	13.41	12.72	4.06	9.42	7.31
42.1	2	0.73	0.45	15.55	0.07	0.037	0.37	90	13.01	14.41	3.65	10.57	8.91
44.0	2	0.70	0.41	16.20	0.07	0.035	0.30	70	11.00	13.98	2.90	10.61	9.51
45.4	2	0.64	0.40	16.10	0.06	0.031	0.25	120	11.09	16.13	2.25	10.71	9.58
47.0	2	0.73	0.38	16.55	0.08	0.036	0.38	70	11.37	17.15	3.07	9.00	8.81
48.4	2	0.48	0.31	17.50	0.05	0.020	0.19	60	9.17	20.29	3.22	7.74	8.41
55.4	3	0.17	17.70	9.42	0.02	0.007	0.06	30	21.18	26.42	6.90	58.82	11.87

Computing method of Mo_{EF}, U_{EF}, and V_{EF}: $X_{EF} = (X/Al_{sample})/(X_{PAAS}/Al_{PAAS})$, where PAAS, indicates post-Archean Australian shales (Taylor and McLennan, 1986).

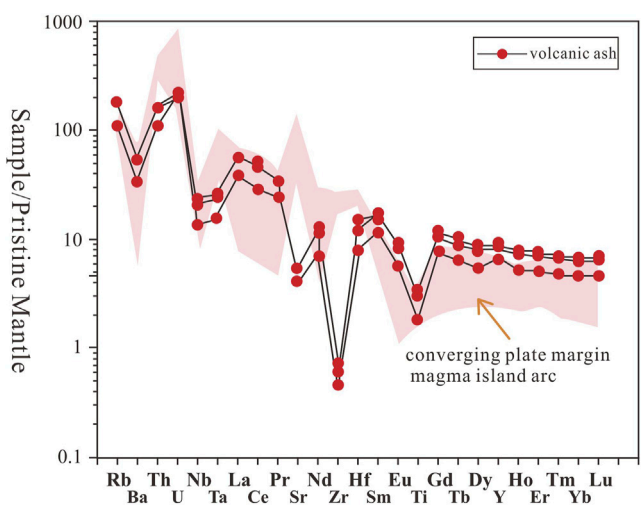

FIGURE 5 | Spider diagram after mantle normalization of the elements in volcanic ash in the Lengshuixi section of the Maokou Formation. Convergent plate marginal magmatic island arc data are taken from Huang et al., 2018).

REE pattern with enriched light REEs, depleted heavy REEs, and negative Eu anomaly (**Figure 6D**) indicates evident plagioclase fractional crystallization before magmatic exhalation, which also indicate the acidic magma eruption (Rollison et al., 2000). Negative Sr, Ti, Ba, and P anomalies in the spider diagram of incompatible elements after primitive mantle normalization (**Figure 5**) indicate a lot of feldspar, apatites, and titanomagnetite detached by magma splitting to finally form rhyolites (Xu et al., 2010). The crossplot of Nb/Y-Zr/TiO_2 also indicates the zone of rhyodacite/dacite (**Figure 7**), which agrees with the conclusion of Middle Permian eruptive rock types in Zhou et al. (2020).

Elements of volcanic ash may also contain implicit information of geological settings. The La/Nb value of 2.24–2.77 is much higher than the value of 0.94 on average (**Table 4**) in the primitive mantle and slightly higher than the value of 2.2 in the continental crust (Saunders et al., 1988). Enriched LIL elements and depleted HFS elements represent the geochemical features similar to island arc/epicontinental arc volcanic rocks relative to the subduction effect (**Figure 5**). The crossplot of Zr-Ti indicates the distribution of these elements in arc magmas (**Figure 7**). Thus, it was concluded that magma origin is related to oceanic crust subduction.

5.2 Terrestrial Environment Change Indicated by Terrestrial Input Before and After a Volcanic Eruption

Terrestrial input index is a good indicator in land ecosystem and tectonic activity. Physical and chemical weathering intensity in a source area for shale depositions are represented using ∑REE and the ratios of Rb/Sr and Rb/Y, respectively, where the higher value corresponds to the more intense weathering (Chen et al., 1999; Wei et al., 2001; Jin et al., 2006). Terrestrial input indicators include Al, Ti, Hf, Nb, Sn, Ta, Th, and Zr, which indicate a small degree of activity and less liable to move from

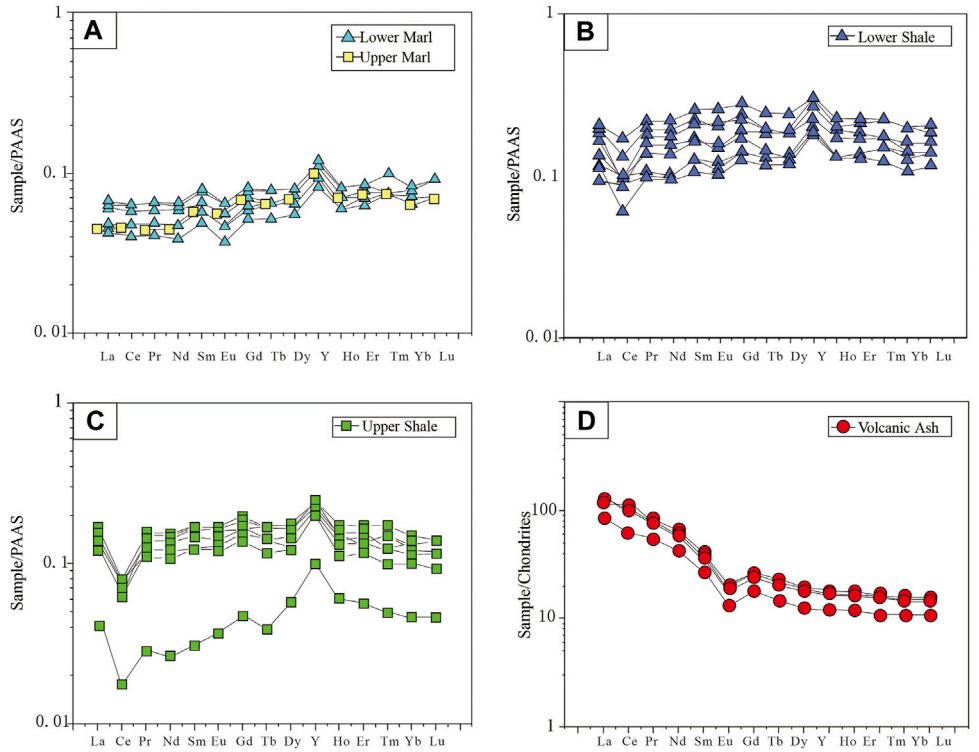

FIGURE 6 | REE patterns of the volcanic ash and overlying and underlying rocks in the Lengshuixi section of the Maokou Formation. PAAS represents post-Archean Australian shales with their REE data taken from Taylor and McLennan (1986); chondrite REE data are taken from Boynton (1984) **(A)**. low and upper marl; **(B)**.lower shale; **(C)**.upper shale; **(D)**.volcanic ash.

volcanic ash into sea water (Zielinski, 1985; Hints et al., 2015; Kiipli et al., 2017).

The ∑REE content and Rb/Sr value increases in the underlying shale layer (**Figure 3C**), which indicates intensified the physical weathering and chemical weathering on land. It is unusual to observe this slight increase in the contents of immobile elements, e.g., Al, Ti, Hf, Nb, Ta, and Zr (**Figure 3C**), because immobile elements tend not to move from volcanic ash into surrounding formations (Hints et al., 2015; Liao, 2020). Such a trend of increasing in the underlying layer indicates the effect from the intensified terrestrial input instead of volcanic ash alteration. This corresponds with our observation of intensified terrestrial input into the Permian Period microbialite underlying layer of volcanic ash (Liao, 2020).

In fact, the volcanic ash beds originated from an island arc eruption. There may be related to the epicontinental uplift (Fisher and Smith, 1991; Sak et al., 2009; Di Capua and Scasso, 2020) and earthquakes (López et al., 2012) before an island arc eruption. For example, precursory monitoring of the 2011 volcanic eruption in El Hierro, Spain, recorded 10,000 earthquakes with the largest surface deformation exceeding 5 cm before the volcanic eruption (López et al., 2012). Land uplift and earthquakes will intensify the terrestrial input effect (Crisafulli and Dale, 2018), and the product of terrestrial input will migrate into the ocean via geologic processes (Xu et al., 2009). Coincidentally, the underlying shale layer shows obviously higher La_N/Sm_N, indicating a degree of light-middle REE enrichment, which denotes an intensified river input, compared to the overlying shale layer (**Table 3**; **Figures 6B,C**). This implies that mass terrestrial materials in the weathered zone were transported by rivers to the ocean, resulting in more terrestrial input into the underlying shale layer of volcanic ash (**Figure 8A**).

Smaller ∑REE, Zr/Y and Rb/Sr in the overlying shale layer, than in the underlying shale layer (**Figure 3C**), indicates declined weathered input. A land ecosystem tends to be seriously destroyed by a volcanic eruption, which will then enhance subsequent terrestrial input. Liao (2020) discovered mass extinction of terrestrial biota and significantly increased terrestrial input on the volcanic ash deposits at the transition from the Permian to the Triassic Period. However, this study of the Maokou Formation observed a significant decrease in volcanic eruption. This may be attributed to a small-scale eruption which did not remarkably alter the land ecosystem. N.N. Li (2020) observed sporopollenin and found basically unchanged arboreal sporopollen and shrubby sporopollen, slightly increased sedgy pollen, and notably increased sphagnum after the volcanic eruption in the Holocene Epoch of northeast China. This implies that volcanic eruptions do not ruin land ecosystems but instead promote plant growth (**Figure 8B**). As a result, the bloom of land plants surpassed the weathering effect in the land-source area. It should be noted that the area of interest was less affected by the volcanic eruption

TABLE 3 | REE contents and representative element ratios in the upper and lower marl and shale layers, the Lengshuixi section.

Thickness (cm)	Lithology	La	Ce	Pr	Nd	Sm	Eu	Gd	Tb	Dy	Y	Ho	Er	Tm	Yb	Lu	∑REE	Ce/ Ce*	Eu/ Eu*	La_N/ Sm_N	Zr/ Y	Rb/ Sr
1.9	1	2.3	4.6	0.52	2.0	0.36	0.06	0.33	0.05	0.34	2.9	0.07	0.22	0.03	0.20	0.03	14.0	0.97	0.02	0.93	3.79	0.01
7.4	1	2.4	5.0	0.57	2.1	0.42	0.07	0.36	0.06	0.38	3.0	0.08	0.24	0.04	0.23	0.04	15.0	0.98	0.02	0.83	3.67	0.00
12.0	1	2.5	5.0	0.58	2.2	0.44	0.07	0.37	0.06	0.37	3.2	0.08	0.24	0.03	0.22	0.04	15.4	0.96	0.02	0.83	2.81	0.00
15.1	1	1.7	3.7	0.43	1.6	0.32	0.05	0.27	0.05	0.30	2.5	0.06	0.20	0.03	0.20	0.03	11.4	0.99	0.01	0.78	4.00	0.00
18.5	1	1.8	3.8	0.43	1.6	0.32	0.05	0.29	0.05	0.30	2.5	0.07	0.20	0.03	0.20	0.03	11.7	0.99	0.01	0.82	4.00	0.00
22.0	1	1.6	3.2	0.36	1.3	0.27	0.04	0.24	0.04	0.26	2.2	0.06	0.18	0.03	0.18	0.03	10.0	0.97	0.01	0.87	4.09	0.01
24.0	2	3.6	6.9	0.88	3.3	0.71	0.13	0.65	0.10	0.63	4.8	0.13	0.39	0.06	0.36	0.06	22.7	0.89	0.06	0.74	3.13	0.17
25.2	2	4.4	8.0	0.94	3.4	0.69	0.12	0.65	0.10	0.61	5.4	0.13	0.38	0.06	0.39	0.06	25.3	0.90	0.06	0.93	3.15	0.15
26.8	2	4.3	4.8	0.86	3.2	0.59	0.11	0.58	0.09	0.55	5.0	0.13	0.39	0.06	0.36	0.06	21.1	0.57	0.05	1.06	3.20	0.14
28.0	2	7.0	6.7	1.38	5.2	0.94	0.16	0.89	0.14	0.91	8.1	0.20	0.60	0.09	0.55	0.09	33.0	0.49	0.11	1.09	3.09	0.16
29.4	2	7.5	10.5	1.72	6.5	1.23	0.22	1.11	0.15	0.85	7.2	0.19	0.52	0.07	0.45	0.07	38.3	0.67	0.19	0.89	2.78	0.30
30.8	2	5.1	7.7	1.22	4.6	0.89	0.17	0.80	0.11	0.59	5.1	0.13	0.37	0.05	0.30	0.05	27.2	0.71	0.10	0.84	2.75	0.24
32.1	2	7.8	13.4	1.91	7.4	1.42	0.28	1.31	0.19	1.13	8.2	0.22	0.64	0.09	0.56	0.08	44.6	0.80	0.28	0.80	2.56	0.38
33.9	2	6.3	7.6	1.56	5.9	1.16	0.23	1.04	0.15	0.87	6.1	0.17	0.48	0.07	0.40	0.06	32.1	0.56	0.18	0.79	2.62	0.29
41.0	3	6.0	6.1	1.33	4.9	0.88	0.18	0.85	0.13	0.75	6.6	0.15	0.45	0.05	0.37	0.06	28.8	0.50	0.11	1.00	2.42	0.23
42.1	3	6.3	5.6	1.38	5.2	0.94	0.18	0.91	0.13	0.76	6.0	0.15	0.37	0.06	0.36	0.06	28.4	0.44	0.12	0.98	2.33	0.13
44.0	3	5.2	4.9	1.07	4.0	0.69	0.13	0.64	0.09	0.57	5.4	0.11	0.33	0.04	0.28	0.04	23.5	0.48	0.06	1.10	2.41	0.13
45.4	3	5.9	4.9	1.24	4.6	0.82	0.15	0.77	0.11	0.57	5.5	0.13	0.38	0.05	0.32	0.05	25.5	0.42	0.09	1.05	2.18	0.11
47.0	2	6.4	6.2	1.32	5.0	0.93	0.17	0.76	0.13	0.82	6.5	0.17	0.49	0.07	0.42	0.06	29.4	0.49	0.10	1.01	2.15	0.17
48.4	2	1.7	1.4	0.25	0.9	0.17	0.04	0.22	0.03	0.27	2.7	0.06	0.16	0.02	0.13	0.02	8.1	0.48	0.01	1.46	2.96	0.13
55.4	3	1.7	3.6	0.39	1.5	0.32	0.06	0.32	0.05	0.32	2.7	0.07	0.21	0.03	0.18	0.03	11.5	1.02	0.01	0.78	1.11	0.00

Ce/Ce = 2CeN/(LaN + PrN); Eu/Eu* = 2EuN/(SmN + GdN). Post-Archean Australian standardized data are taken from Taylor and McLennan (1986).*

TABLE 4 | REE contents and representative element ratios in the volcanic ash layer, the Lengshuixi section.

Thickness	Lithology	La	Ce	Pr	Nd	Sm	Eu	Gd	Tb	Dy	Y	Ho	Er	Tm	Yb	Lu	∑REE	La_N/Yb_N	La/Nb	Eu/Eu*	Zr/Y	Rb/Sr
35.1	3	39.5	81.8	10.00	38.5	7.95	1.50	6.87	1.01	6.04	40.7	1.19	3.40	0.50	3.01	0.47	242.4	8.85	2.58	0.61	3.34	1.08
36.9	3	37.6	90.2	9.57	36.0	7.43	1.48	6.83	1.09	6.22	41.3	1.28	3.66	0.52	3.28	0.51	247.0	7.73	2.54	0.62	3.70	1.04
38.1	3	37.7	82.6	9.40	34.6	6.99	1.35	6.16	0.95	5.77	38.8	1.19	3.42	0.50	3.08	0.47	233.0	8.25	2.24	0.62	4.51	1.07
39.8	3	26.6	50.6	6.72	25.4	5.26	0.96	4.62	0.69	3.97	30.2	0.86	2.47	0.35	2.26	0.35	161.3	7.94	2.77	0.58	3.15	0.84

$Eu/Eu^* = 2Eu_N/(Sm_N + Gd_N)$. Standardized chondrite data are taken from Boynton (1984).

due to the long distance from the crater, which cannot be excluded from the results.

5.3 Bio-Precursor Change During and After Volcanic Eruption

Volcanic eruptions bring forth wildfires and elementary substances, which may change ocean and land ecosystems (Cui et al., 1997; Crisafulli and Dale, 2018) and consequently the bio-precursor types. HI and OI could be used to indicate the change of the bio-precursor type in sediments. HI denotes hydrogen richness in organic matter, and OI denotes oxygen richness in organic matter. A high HI indicates strong hydrocarbon generation capacity. For example, bacteria and algae with high lipid content exhibits high HI. A high OI indicates poor hydrocarbon generation capacity. High content of terrestrial plants corresponds to high OI. Thus, we could use HI and OI to estimate the change in source organism type/organic matter type (Peters et al., 2005).

Volcanic ash-I feature increased OI and decreased HI (**Figure 3A**). The increase in OI is dominated by volcanic eruption-induced wildfires, which causes leaves to drop and trees to burn (Cui et al., 1997). A large amount of land plant fragments is transported by air or rivers to oceans, which increases the content of terrestrial organic matter in an ocean (Scott, 2010) (**Figure 8C**). This causes a sharp reduction in the biodiversity of an ocean (Hints et al., 2003; Perrier et al., 2012) and when organisms die, many corrosive animals first migrate into this area (Walker et al., 2013). Organic matter is consumed and not preserved in the formations (**Figure 8C**), eventually leading to increased OI and decreased HI.

Volcanic ash-II eruptions feature increased HI, and decreased OI, which are attributed to zero terrestrial organic matter transportation from the land. The existence of residual organisms, like algae in the ocean (Walker et al., 2013) (**Figure 8D**), give rise to increased HI and decreased OI.

However, a HI of 2.6 and OI of 10.5, on average, in the overlying shale layer are similar to the HI of 3.9 and OI of 11.2, on average, in the underlying shale layer. This mostly likely indicates a zero change in source organism type in the shales after a volcanic eruption. In fact, the land and ocean ecosystems may quickly recover after a volcanic eruption. A plankton and benthos food chain in the ocean could be rebuilt within a few years, and remnant land plants could be revitalized in less than 2 years (DeGange et al., 2010). Therefore, consistent HI and OI in underlying and overlying shale sediments may be related to regenerating organic matter in ocean and land environments. (**Figure 8B**).

5.4 Volcanic Action on Organic Matter Enrichment and Its Mechanism

5.4.1 Influence on Organic Matter Content Content and Vertical Range of Influence

HI and OI almost remain unchanged in the overlying shales, but further discussion on the volcanic ash effect on the TOC content is needed. Compared with the underlying shale layer, the

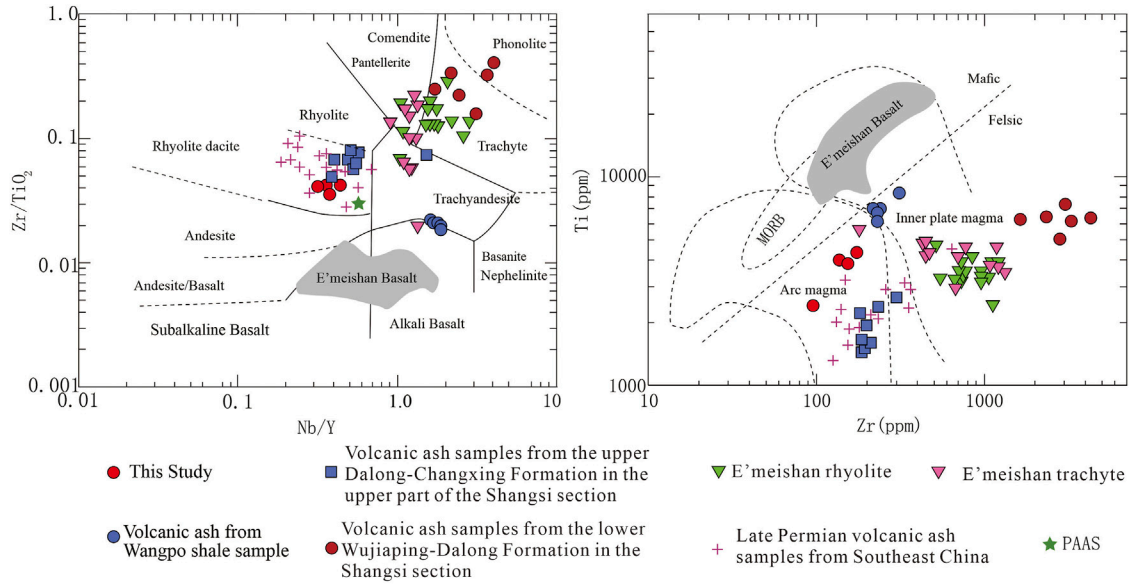

FIGURE 7 | Nb/Y-Zr/TiO_2 (Winchester and Floyd, 1977) and Zr-Ti (Pearce, 1982) crossplots for volcanic ash samples from the Lengshuixi section in the Maokou Formation [reproduced from Huang et al. (2018)]. Wangpo-shale volcanic ash data was taken from (Pearce, 1982); the data of the volcanic ash from the Wujiaping-Changxing Formations in the Shangsi section was taken from Huang et al. (2018); the data of rhyolites and trachytes from the Emei Mountain were taken from Xu et al. (2001), Fan et al. (2008), He et al. (2010), Qi et al. (2008), Xiao et al. (2003), Xiao et al. (2004); the data of the last-phase volcanic ash from the Upper Permian Series in southeast China was obtained from Liao et al. (2016a), Liao et al. (2016b); post-Archean Australian shale data was taken from McLennan (2018).

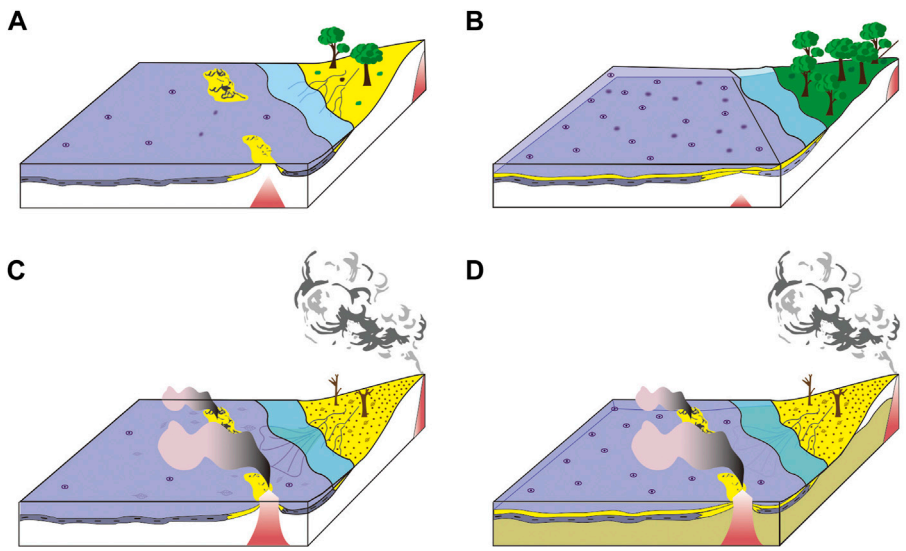

FIGURE 8 | Mechanism of a volcanic action on organic matter enrichment in a neritic carbonate platform environment. **(A)** Topographic rise, enhanced earthquakes, and more terrestrial inputs before a volcanic eruption. **(B)** Synergistically increased ocean and land productivity after a volcanic eruption. **(C)** Land plants die and consequently increase input of terrestrial organic matter in phase-I of a volcanic eruption. **(D)** Decreased input of terrestrial organic matter and remnant organisms, like algae, in phase-II of a volcanic eruption.

overlying shale layer shows increased TOC content by 18% (**Figure 3A**). In the vertical direction, the TOC content significantly decreases in the upper level of the overlying shale layer (**Figure 3A**), which means that the largest range of influence doubles the thickness of the volcanic ash layer.

To clarify, further assessment is needed to determine if the TOC content in the underlying shale layer should be used as a background value because the TOC in this layer may be diluted by increased terrestrial inputs at the dispositional stage of shales. As for underlying shale samples, the TOC content hardly decreases with

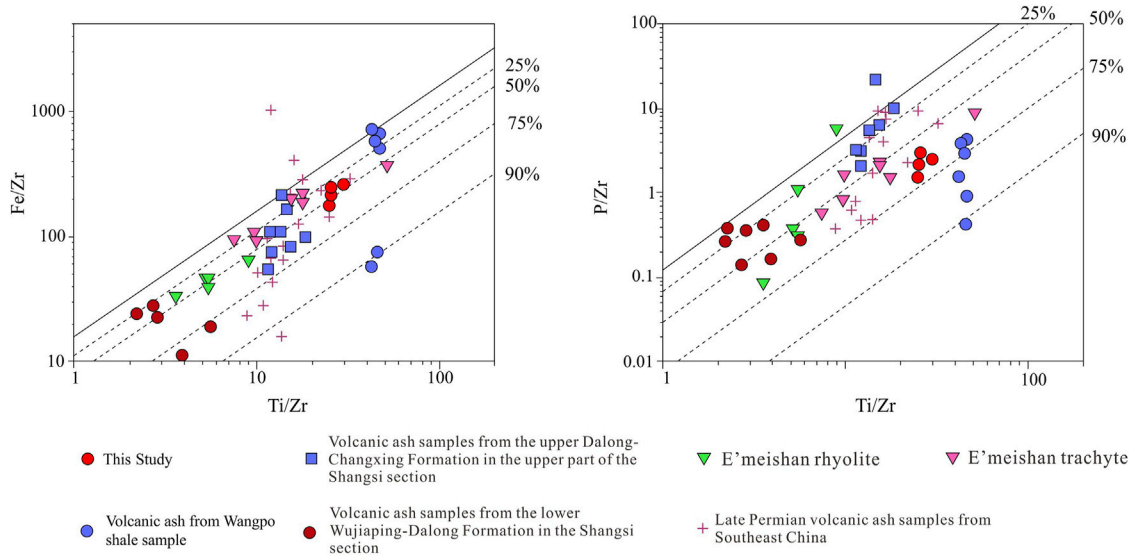

FIGURE 9 | Nutritive element loss based on intrusive rock data from south China [after Zhao et al. (2020)]. Black lines indicate plutonite data from the South China plate; four dotted lines indicate the loss of 25, 50, 75%, and 90, respectively. Wangpo-shale volcanic ash data was taken from Huang et al. (2016); the data for the volcanic ash from the Wujiaping-Changxing Formations in the Shangsi section was taken from Huang et al. (2018); the data of rhyolites and trachytes from the Emei Mountain were taken from Xu et al. (2010); the data from the last-phase volcanic ash of the Upper Permian Series in southeast China, was taken from (Liao et al., 2016a; Liao et al., 2016b); and post-Archean Australian shale data was taken from McLennan (2018).

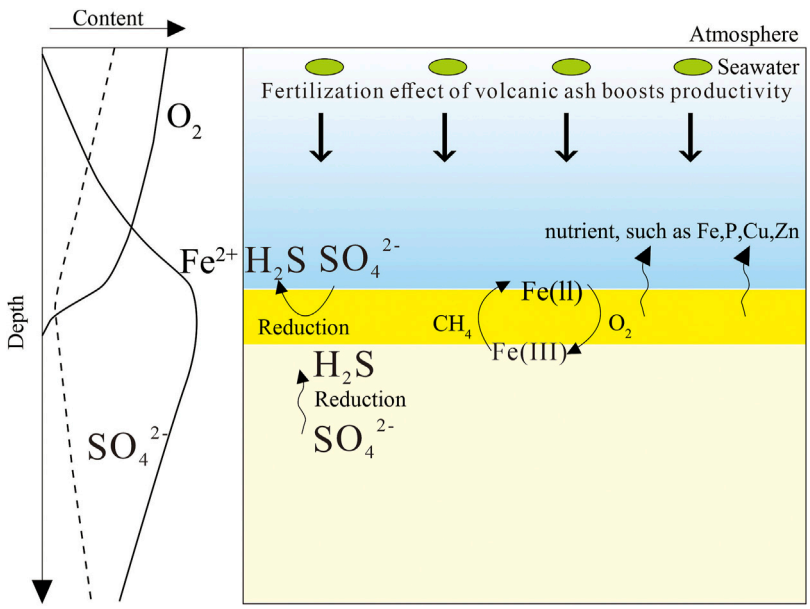

FIGURE 10 | Schematic element movement, chemical reactions, and the effects on productivity and oxidation-reduction conditions close to the volcanic ash layer.

∑REE content, Rb/Sr, and the content of immobile elements (**Figure 3**). This confirms the findings that terrestrial inputs were not sufficient enough to significantly alter the TOC content in the underlying shale layer at its depositional stage. Thus, it is appropriate to use the TOC content in the underlying shale layer as a background value to estimate TOC increment by volcanic ash.

5.4.2 Volcanic Ash Nourishment for Organism Growth

Increased TOC content in the overlying shale layer was related to improved paleoproductivity. Studies show that modern eruptive volcanic ash contains many nutritive elements, including volatile compounds, e.g., NH_4^+, NO_3^-, PO_4^{3-}, and SiO_2, and trace elements, e.g., Al, Cd, Co, Cu, Mn, Ni, Pb, and Zn (Frogner

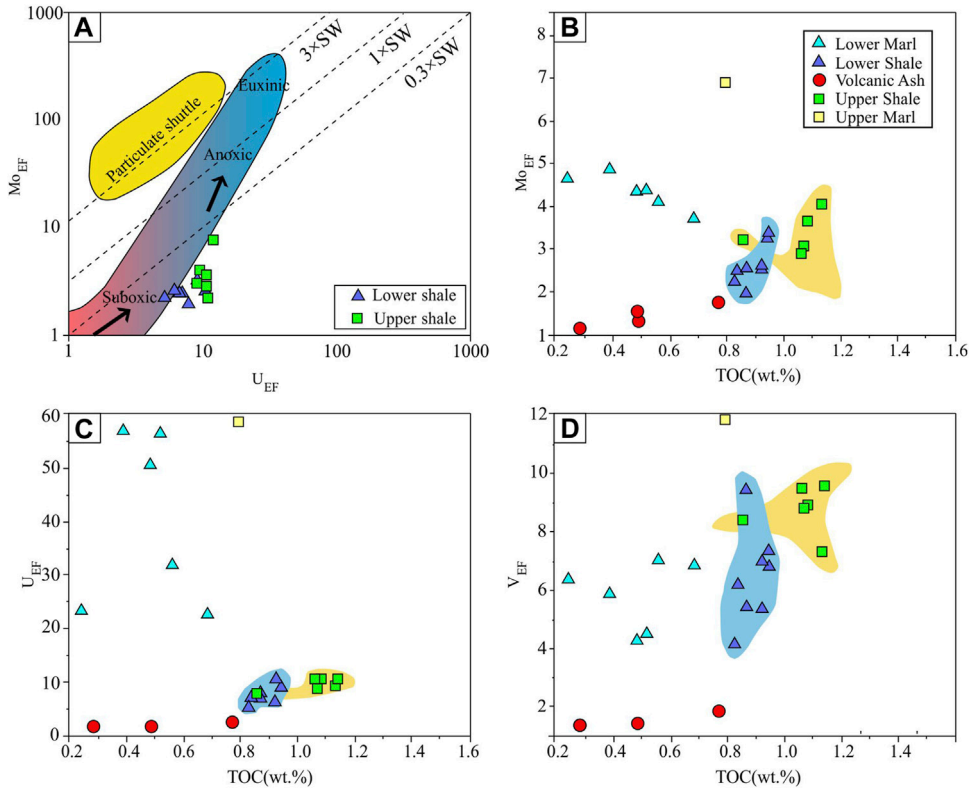

FIGURE 11 | Crossplots of **(A)** MoEF vs UEF, **(B)** TOC vs MoEF, **(C)** TOC vs UEF, and **(D)** TOC vs VEF. Three dotted lines in **(A)** represent that the Mo_{EF}/U_{EF} has a value of 0.3, 1, and 3 times that of sea water. The zone with graduated color indicates U-Mo covariance in a normal open ocean environment, and the green zone indicates U-Mo covariance with the effect of metal particle carriers [modified from Algeo and Tribovillard (2009)].

et al., 2001; Witham et al., 2005; Frogner Kockum et al., 2006; Duggen et al., 2007; Jones and Gislason, 2008). In particular, the element Fe, may greatly promote productivity (Zeng et al., 2018) because the oceans in geologic history usually assumed Fe deficiency (Duggen et al., 2010). This study showed much higher Fe content in volcanic ash than in overlying and underlying shales of the volcanic ash layer (**Figure 3B**). **Figure 9** shows a Fe loss of 50%, which agrees with the results of Lee et al. (2018) and Zhao et al. (2020). This means Fe in volcanic ash travelled into the iron-deficient environment Lee et al. (2018).

Element P, is a basic element of marine plankton and an important component of all organisms. P is widely used as a paleoproductivity indicator (Hints et al., 2015). **Figure 9** shows P loss of over 75% in volcanic ash. Fe and P migrating from the volcanic ash layer into the overlying shale layer may boost the productivity in the overlying layer.

In addition, important micronutrients (e.g., Cu and Zn) in the ocean, are also limited-elements which could extensively stimulate ocean productivity and plankton accumulation (Brumsack, 2006). The ratio of element to Al could be used to exclude the effect of terrestrial input. For example, Cu/Al and Zn/Al. The Cu/Al value is obviously higher in the overlying shale layer than in the underlying shale layer (**Figure 3B**). The value of Zn/Al in the overlying shale layer increases with the distance to volcanic ash within 8 cm (**Figure 3B**), which is in agreement with the thickness of TOC increment. This means that in addition to terrestrial input, some Cu and Zn originated from volcanic ash and were re-deposited in water. In addition to increased Cu and Zn in volcanic ash observed in this study, Hints et al. (2015) observed remarkably increased P and Ca in the marls above bentonite, and Wang et al. (2021) showed increased P, Ni, and Cu in the shale layer above the volcanic ash layer. All these elements could improve paleoproductivity (Hints et al., 2015; Wang et al., 2021).

The moss sample from volcanic ash was compared with the analogues from shales to further confirm the direct effect of elements on plant growth. Moss is a transition group from aquatic plants to terrestrial plants. As per outcrop observation, the moss was more flourishing in volcanic ash than in the overlying and underlying mud shales (**Figure 2**). In accordance with the comparative study of the essential elements in moss, i.e., Ca, Mg, K, Fe, P, S, and Mn, additional element content was higher in the moss sample from volcanic ash than in the analogues from overlying and underlying shales, except S (low S content in volcanic ash) (**Figure 4**).

The essential elements mainly originate from atmospheric sedimentation and growth matrix. The former mainly includes atmospheric precipitation with dry (humid) dust fall, and the latter includes rocks and soil (Tuttle et al., 1986). The element discrepancies between two moss samples, with a difference of length in growth to be less than 1 m, and these are obviously related to growth matrix instead of atmospheric sedimentation.

Further, **Figure 3B** shows that volcanic ash accumulates these essential elements. This means that moss growth was promoted by high-content essential elements migrating from volcanic ash into moss plants. Therefore, it can be inferred that volcanic action on TOC enrichment may be attributed to enough essential elements in volcanic ash for plant or algae growth and metabolism. It is worth mentioning that, with the existing means, we're not sure that nutrients in volcanic ash are is the only sole thing trigger that could boost moss growth because the ash has higher permeability and moisture content.

5.4.3 Volcanic Ash Effect on Oxidation-Reduction

Volcanic ash may change the redox properties of sediments. After volcanic ash deposition, Fe^{2+} generated by volcanic ash bonded with silicate and oxidized by O_2 will form Fe^{3+} and $Fe(OH)_3$ precipitates. In this process, O_2 in and below volcanic ash will be consumed sharply (Hembury et al., 2012) and even exhausted when the volcanic ash layer is thicker than 3 cm (Haeckel et al., 2001). After that, $Fe(OH)_3$ will function as the oxidizing agent to oxidize methane, when methane is produced. Meanwhile, $Fe(OH)_3$ itself will be reduced into Fe^{2+} ($CH_4 + 8Fe(OH)_3 + 15H^+ \rightarrow HCO_3^- + 8Fe^{2+} + 21H_2O$) (Luo et al., 2020) and go into water column once again (**Figure 10**).

Water column of the volcanic ash may also be affected by volcanic ash. **Figure 3A** shows quickly declining TS content in the volcanic ash layer as well as in the overlying and underlying shale layers. Subsurface sulfur elements usually turn up in the forms of elemental sulfur, sulfates, disulfides, and compounds bonded with organic matter (Tuttle et al., 1986). Sulfur will be consumed by sulfate reducing bacteria in a reducing condition ($2CH_2O + SO_4^{2-} \rightarrow 2HCO_3^- + H_2S$) (Boetius et al., 2000). In the shallow oxidized carbonate platform, volcanic ash provides a reducing condition for sulfate reaction (**Figure 10**), which led to the decrease in TS content in the overlying and underlying layers of volcanic ash. Organic matter enrichment was more affected by volcanic ash in the overlying shale layer than in the underlying shale layer because underlying shales were in an oxidizing environment at the depositional stage, whereas overlying shales had already been affected by volcanic ash at the depositional stage.

The difference between Mo_{EF} enrichment and U_{EF} enrichment, in different reducing conditions, could be used to indicate the oxidation-reduction conditions at the depositional stage (Algeo and Tribovillard, 2009). **Figure 11A** shows that samples from the overlying shale layer were closer to anoxic water which indicates that overlying shales were in a more reducing environment at the depositional stage and such an environment was favorable for organic matter enrichment. The crossplots of TOC content and Mo_{EF}, U_{EF}, and V_{EF} show that the TOC content is higher in the overlying shale layer than in the underlying shale layer (**Figure 3B**; **Figures 11B,C**).

6 CONCLUSION

Based on outcrop, mineralogical, organic geochemical, and inorganic geochemical studies three conclusions can be determined:

1) Terrestrial inputs increase before a volcanic eruption and decrease after an eruption due to land ecosystem recovery and plant growth promoted by volcanic ash as a nutritive substance.
2) Plant fragments migrate to water at the beginning of a volcanic eruption, which results in poor organic matter type. At the end of a volcanic eruption, there is less input of plant fragments and organic matter mainly originating from bacteria and algae, which resulted in a good organic matter type.
3) Volcanic ash may increase the TOC content by 18%, and the range of influence doubled the thickness of the volcanic ash layer. Such effects were related to the fact that volcanic ash offered nutritive elements and altered the redox conditions of water (Xu et al., 2009).

DATA AVAILABILITY STATEMENT

The original contributions presented in the study are included in the article/Supplementary Material, further inquiries can be directed to the corresponding authors.

AUTHOR CONTRIBUTIONS

QM raised the key issues of this study, collected samples, interpreted the analysis data, and formed a draft outline. QP collected samples, conducted analytical tests, and wrote drafts. GH chose the field outcrop, analyzed the source of the volcanic ash, and formed a draft outline. ZJ proposed revisions to the full text, and initially established the influencing model. DZ carried out SEM analysis of reservoir physical properties and quartz. JL participated in field work and drew some drawings. CZ organized the analysis data and drew some graphs.

FUNDING

This work was jointly funded by the National Natural Science Foundation of China (Nos 41872164, 41872155,41930426 and 42172168) as same as State Key Laboratory of Organic Geochemistry, GIGCAS (Grant No. 2125).

ACKNOWLEDGMENTS

We thank Zhang Shuichang, Wang Huajian and Wang Xiaomei of PetroChina Research Institute of Petroleum Exploration and Development for their support in field section positioning and field discussion. We also thank Song Daofu of China University of Petroleum (Beijing) for analysis and test of TOC and rock pyrolysis. The authors appreciate the previewers, that is, Prof. Fujiang Jiang from China University of Petroleum, Beijing and Dr. Xiaoqiang Li from Texas Tech University, USA, who give constructive suggestion which polish the paper so much.

REFERENCES

Algeo, T. J., and Tribovillard, N. (2009). Environmental Analysis of Paleoceanographic Systems Based on Molybdenum-Uranium Covariation. *Chem. Geology.* 268, 211–225. doi:10.1016/j.chemgeo.2009.09.001

Boetius, A., Ravenschlag, K., Schubert, C. J., Rickert, D., Widdel, F., Gieseke, A., et al. (2000). A marine Microbial Consortium Apparently Mediating Anaerobic Oxidation of Methane. *Nature* 407, 623–626. doi:10.1038/35036572

Boynton, W. V. (1984). *Cosmochemistry of the Rare Earth Elements: Meteorite Studies, Developments in Geochemistry*. Elsevier, 63–114. doi:10.1016/b978-0-444-42148-7.50008-3

Brumsack, H.-J. (2006). The Trace Metal Content of Recent Organic Carbon-Rich Sediments: Implications for Cretaceous Black Shale Formation. *Palaeogeogr. Palaeoclimatol. Palaeoecol.* 232, 344–361. doi:10.1016/j.palaeo.2005.05.011

Cannata, C. B., De Rosa, R., Donato, P., Donato, S., Lanzafame, G., Mancini, L., et al. (2019). First 3D Imaging Characterization of Pele's Hair from Kilauea Volcano (Hawaii). *Sci. Rep.* 9, 1–13. doi:10.1038/s41598-018-37983-9

Chen, J., An, Z., and Head, J. (1999). Variation of Rb/Sr Ratios in the Loess-Paleosol Sequences of central China during the Last 130,000 Years and Their Implications for Monsoon Paleoclimatology. *Quat. Res.* 51, 215–219. doi:10.1006/qres.1999.2038

C. M. Crisafulli, and V. H. Dale (Editors) (2018). *Ecological Responses at Mount St. Helens: Revisited 35 Years after the 1980 Eruption* (Springer).

Cui, Z. X., Zhang, S. H., and Tian, J. (1997). The Study on Volcanic Eruption and forest Conflagration in Changbai Mountain since Holocene Quaternary. *Geographical Res.* 1, 92–97.

DeGange, A. R., Byrd, G. V., Walker, L. R., and Waythomas, C. F. (2010). Introduction-The Impacts of the 2008 Eruption of Kasatochi Volcano on Terrestrial and Marine Ecosystems in the Aleutian Islands, Alaska. *Arctic, Antarctic, Alpine Res.* 42, 245–249. doi:10.1657/1938-4246-42.3.245

Di Capua, A., and Scasso, R. A. (2020). Sedimentological and Petrographic Evolution of a Fluvio-Lacustrine Environment during the Onset of Volcanism: Volcanically-Induced Forcing of Sedimentation and Environmental Responses. *Sedimentology* 67, 1879–1913. doi:10.1111/sed.12681

Duffield, W. A., Gibson, E., and Heiken, G. (1977). Some Characteristics of Pele's Hair. *J. Res. US Geol. Surv.* 5, 93–101.

Duggen, S., Croot, P., Schacht, U., and Hoffmann, L. (2007). Subduction Zone Volcanic Ash Can Fertilize the Surface Ocean and Stimulate Phytoplankton Growth: Evidence from Biogeochemical Experiments and Satellite Data. *Geophys. Res. Lett.* 34, 1–5. doi:10.1029/2006GL027522

Duggen, S., Olgun, N., Croot, P., Hoffmann, L., Dietze, H., Delmelle, P., et al. (2010). The Role of Airborne Volcanic Ash for the Surface Ocean Biogeochemical Iron-Cycle: a Review. *Biogeosciences* 7, 827–844. doi:10.5194/bg-7-827-2010

Fan, W., Zhang, C., Wang, Y., Guo, F., and Peng, T. (2008). Geochronology and Geochemistry of Permian Basalts in Western Guangxi Province, Southwest China: Evidence for Plume-Lithosphere Interaction. *Lithos* 102, 218–236. doi:10.1016/j.lithos.2007.09.019

Fisher, R. V., and Smith, G. A. (1991). "Volcanism, Tectonics and Sedimentation,". *Sedimentation in Volcanic Settings*. Editors R. V. Fisher, and G. A. Smith (Tulsa, Oklahoma, United States: SEPM Special Publication), 45, 1–5. doi:10.2110/pec.91.45.0001

Frogner Kockum, P. C., Herbert, R. B., and Gislason, S. R. (2006). A Diverse Ecosystem Response to Volcanic Aerosols. *Chem. Geology.* 231, 57–66. doi:10.1016/j.chemgeo.2005.12.008

Frogner, P., Reynir Gíslason, S., and Óskarsson, N. (2001). Fertilizing Potential of Volcanic Ash in Ocean Surface Water. *Geol* 29, 487–490. doi:10.1130/0091-7613(2001)029<0487:fpovai>2.0.co;2

Gao, P., He, Z., Lash, G. G., Li, S., Xiao, X., Han, Y., et al. (2020). Mixed Seawater and Hydrothermal Sources of Nodular Chert in Middle Permian limestone on the Eastern Paleo-Tethys Margin (South China). *Palaeogeogr. Palaeoclimatol. Palaeoecol.* 551, 109740. doi:10.1016/j.palaeo.2020.109740

Guoheng Liu, G., Zhai, G., Huang, Z., Zou, C., Xia, X., Shi, D., et al. (2019). The Effect of Tuffaceous Material on Characteristics of Different Lithofacies: A Case Study on Lucaogou Formation fine-grained Sedimentary Rocks in Santanghu Basin. *J. Pet. Sci. Eng.* 179, 355–377. doi:10.1016/j.petrol.2019.04.072

Haeckel, M., van Beusekom, J., Wiesner, M. G., and König, I. (2001). The Impact of the 1991 Mount Pinatubo Tephra Fallout on the Geochemical Environment of the Deep-Sea Sediments in the South China Sea. *Earth Planet. Sci. Lett.* 193, 151–166. doi:10.1016/S0012-821X(01)00496-4

He, Q., Xiao, L., Balta, B., Gao, R., and Chen, J. (2010). Variety and Complexity of the Late-Permian Emeishan Basalts: Reappraisal of Plume-Lithosphere Interaction Processes. *Lithos* 119, 91–107. doi:10.1016/j.lithos.2010.07.020

Hembury, D. J., Palmer, M. R., Fones, G. R., Mills, R. A., Marsh, R., and Jones, M. T. (2012). Uptake of Dissolved Oxygen during marine Diagenesis of Fresh Volcanic Material. *Geochimica et Cosmochimica Acta* 84, 353–368. doi:10.1016/j.gca.2012.01.017

Hints, O., Hints, L., Sohar, K., and Sohar, K. (2003). Biotic Effects of the Ordovician Kinnekulle Ash-Fall Recorded in Northern Estonia. *Bull. Geol. Soc. Denmark* 50, 115–123. doi:10.37570/bgsd-2003-50-09

Hints, R., Kallaste, T., Kiipli, T., and Siir, S. (2015). Internal Stratification of Two Thick Ordovician Bentonites of Estonia: Deciphering Primary Magmatic, Sedimentary, Environmental and Diagenetic Signatures. *Estonian J. Earth Sci.* 64, 140–158. doi:10.3176/earth.2015.23

Hoffmann, L. J., Breitbarth, E., Ardelan, M. V., Duggen, S., Olgun, N., Hassellöv, M., et al. (2012). Influence of Trace Metal Release from Volcanic Ash on Growth of Thalassiosira Pseudonana and Emiliania Huxleyi. *Mar. Chem.* 132-133, 28–33. doi:10.1016/j.marchem.2012.02.003

Huang, H., Cawood, P. A., Hou, M.-C., Yang, J.-H., Ni, S.-J., Du, Y.-S., et al. (2016). Silicic Ash Beds Bracket Emeishan Large Igneous Province to. *Lithos* 264, 17–27. doi:10.1016/j.lithos.2016.08.013

Huang, H., Cawood, P. A., Hou, M.-C., Ni, S.-J., Yang, J.-H., Du, Y.-S., et al. (2018). Provenance of Late Permian Volcanic Ash Beds in South China: Implications for the Age of Emeishan Volcanism and its Linkage to Climate Cooling. *Lithos* 314-315, 293–306. doi:10.1016/j.lithos.2018.06.009

Ji, R. S., Qin, D. Y., Gao, C. L., Yin, Y., and Fan, X. L. (1997). *East Qinling Orogenic belt and basin*. Xi 'an: Xi 'an Map Publishing House.

Jin, Z., Cao, J., Wu, J., and Wang, S. (2006). A Rb/Sr Record of Catchment Weathering Response to Holocene Climate Change in Inner Mongolia. *Earth Surf. Process. Landforms* 31, 285–291. doi:10.1002/esp.1243

Jingya Zhang, J., Liu, G., Cao, Z., Tao, S., Felix, M., Kong, Y., et al. (2019). Characteristics and Formation Mechanism of Multi-Source Mixed Sedimentary Rocks in a saline lake, a Case Study of the Permian Lucaogou Formation in the Jimusaer Sag, Northwest China. *Mar. Pet. Geology.* 102, 704–724. doi:10.1016/j.marpetgeo.2019.01.016

Jones, M. T., and Gislason, S. R. (2008). Rapid Releases of Metal Salts and Nutrients Following the Deposition of Volcanic Ash into Aqueous Environments. *Geochimica et Cosmochimica Acta* 72, 3661–3680. doi:10.1016/j.gca.2008.05.030

Kiipli, T., Hints, R., Kallaste, T., Verš, E., and Voolma, M. (2017). Immobile and mobile Elements during the Transition of Volcanic Ash to Bentonite - an Example from the Early Palaeozoic Sedimentary Section of the Baltic Basin. *Sediment. Geology.* 347, 148–159. doi:10.1016/j.sedgeo.2016.11.009

Lee, C.-T. A., Jiang, H., Ronay, E., Minisini, D., Stiles, J., and Neal, M. (2018). Volcanic Ash as a Driver of Enhanced Organic Carbon Burial in the Cretaceous. *Sci. Rep.* 8, 4197. doi:10.1038/s41598-018-22576-3

Li Li, L., Liu, Z., Sun, P., Li, Y., and George, S. C. (2020). Sedimentary basin Evolution, Gravity Flows, Volcanism, and Their Impacts on the Formation of the Lower Cretaceous Oil Shales in the Chaoyang Basin, Northeastern China. *Mar. Pet. Geology.* 119, 104472. doi:10.1016/j.marpetgeo.2020.104472

Li, N. N. (2020). *Response of Vegetation Dynamics to Climate Change since the Younger Dryas in the Longgang Region, Northeastern China*. Changchun, China: Northeast Normal University.

Liang, X. P., Jin, Z. J., Liu, Q. Y., Shpilman, A., Li, P., Morozov, V., et al. (2021). Impact of Volcanic Ash on the Formation of Organic-Rich Shale:A Case Study on the Mesozoic Bazhenov Formation,West Siberian Basin. *Oil Gas Geology.* 42, 201–211.

Liao, W. (2020). *Palaeoenvironment Change in Shallow-marine Carbonate Platform across the Permian-Triassic Boundary in South China and its Possible Cause*. Beijing: China University of Geosciences.

Liao, Z., Hu, W., Cao, J., Wang, X., Yao, S., Wu, H., et al. (2016a). Heterogeneous Volcanism across the Permian-Triassic Boundary in South China and Implications for the Latest Permian Mass Extinction: New Evidence from

Volcanic Ash Layers in the Lower Yangtze Region. *J. Asian Earth Sci.* 127, 197–210. doi:10.1016/j.jseaes.2016.06.003

Liao, Z. W., Hu, W. X., Wang, X. L., Cao, J., Yao, S. P., and Wan, Y. (2016b). Volcanic Origin of Claystone Near the Permian-Triassic Boundary in the Deep Water Environment of the Lower Yangtze Region and its Implications for LPME. *Acta Geologica Sinica* 90, 785–800.

Ling, K. Y., Wen, H. J., Zhang, Q. Z., Luo, C. G., Gu, H. N., Du, S. J., et al. (2021). Super-enrichment of Lithium and Niobium in the Upper Permian Heshan Formation in Pingguo,Guangxi, China. *Scientia Sinica(Terrae)* 51, 853–873. doi:10.1007/s11430-020-9752-6

Liu, Y. G., Cao, D. L., Zhang, D. Y., Sun, J. L., Nielsen, O. B., and Shi, F. X. (2007). Holocene Tephra Deposits in the Northern Okinawa Trough. *Adv. Mar. Sci.* 1, 34–45.

Longman, J., Palmer, M. R., Gernon, T. M., and Manners, H. R. (2019). The Role of Tephra in Enhancing Organic Carbon Preservation in marine Sediments. *Earth-Science Rev.* 192, 480–490. doi:10.1016/j.earscirev.2019.03.018

Longman, J., Palmer, M. R., and Gernon, T. M. (2020). Viability of Greenhouse Gas Removal via Artificial Addition of Volcanic Ash to the Ocean. *Anthropocene* 32, 100264. doi:10.1016/j.ancene.2020.100264

López, C., Blanco, M. J., Abella, R., Brenes, B., Cabrera Rodríguez, V. M., Casas, B., et al. (2012). Monitoring the Volcanic Unrest of El Hierro (Canary Islands) before the Onset of the 2011-2012 Submarine Eruption. *Geophys. Res. Lett.* 39, a–n. doi:10.1029/2012GL051846

Luo, M., Torres, M. E., Hong, W.-L., Pape, T., Fronzek, J., Kutterolf, S., et al. (2020). Impact of Iron Release by Volcanic Ash Alteration on Carbon Cycling in Sediments of the Northern Hikurangi Margin. *Earth Planet. Sci. Lett.* 541, 116288. doi:10.1016/j.epsl.2020.116288

Luo, Z. L. (2009). Emei Taphrogenesis and Natural Gas Prospecting Practices in Sichuan Basin. *Xinjiang Pet. Geology.* 30, 419–424.

McLennan, S. M. J. (2018). "Rare Earth Elements in Sedimentary Rocks: Influence of Provenance and Sedimentary Processes," in *Geochemistry and Mineralogy of Rare Earth Elements*, 169–200.

Pearce, J. A. (1982). "Trace Element Characteristics of Lavas from Destructive Plate Boundaries," in *Andesites*. Editor R. S. Thorpe (New York: John Wiley), 525–548.

Perrier, V., Meidla, T., Tinn, O., and Ainsaar, L. (2012). Biotic Response to Explosive Volcanism: Ostracod Recovery after Ordovician Ash-Falls. *Palaeogeogr. Palaeoclimatol. Palaeoecol.* 365-366, 166–183. doi:10.1016/j.palaeo.2012.09.024

Peters, K. E., Peters, K. E., Walters, C. C., and Moldowan, J. (2005). *The Biomarker Guide*. Cambridge University Press.

Qi, L., Wang, C. Y., and Zhou, M.-F. (2008). Controls on the PGE Distribution of Permian Emeishan Alkaline and Peralkaline Volcanic Rocks in Longzhoushan, Sichuan Province, SW China. *Lithos* 106, 222–236. doi:10.1016/j.lithos.2008.07.012

Qing Li, Q., Wu, S., Xia, D., You, X., Zhang, H., and Lu, H. (2020). Major and Trace Element Geochemistry of the Lacustrine Organic-Rich Shales from the Upper Triassic Chang 7 Member in the Southwestern Ordos Basin, China: Implications for Paleoenvironment and Organic Matter Accumulation. *Mar. Pet. Geology.* 111, 852–867. doi:10.1016/j.marpetgeo.2019.09.003

Quanyou Liu, Q., Zhu, D., Jin, Z., Meng, Q., and Li, S. (2019). Influence of Volcanic Activities on Redox Chemistry Changes Linked to the Enhancement of the Ancient Sinian Source Rocks in the Yangtze Craton. *Precambrian Res.* 327, 1–13. doi:10.1016/j.precamres.2019.02.017

Rollison, H. R., Yang, X. M., and Yang, X. Y. (2000). *Rock Geochemistry*. Hefei: Science and Technology of China Press.

Sak, P. B., Fisher, D. M., Gardner, T. W., Marshall, J. S., and LaFemina, P. C. (2009). Rough Crust Subduction, Forearc Kinematics, and Quaternary Uplift Rates, Costa Rican Segment of the Middle American Trench. *Geol. Soc. America Bull.* 121, 992–1012. doi:10.1130/B26237.1

Saunders, A. D., Norry, M. J., and Tarney, J. (1988). Origin of MORB and Chemically-Depleted Mantle Reservoirs: Trace Element Constraints. *J. Pet.* Special_Volume, 415–445. doi:10.1093/petrology/Special_Volume.1.415

Scott, A. C. (2010). Charcoal Recognition, Taphonomy and Uses in Palaeoenvironmental Analysis. *Palaeogeogr. Palaeoclimatol. Palaeoecol.* 291, 11–39. doi:10.1016/j.palaeo.2009.12.012

Shaomin Zhang, S., Cao, Y., Liu, K., Jahren, J., Xi, K., Zhu, R., et al. (2019). Characterization of Lacustrine Mixed fine-grained Sedimentary Rocks Using Coupled Chemostratigraphic-Petrographic Analysis: A Case Study from a Tight Oil Reservoir in the Jimusar Sag, Junggar Basin. *Mar. Pet. Geology.* 99, 453–472. doi:10.1016/j.marpetgeo.2018.10.039

Shellnutt, J. G., and Jahn, B.-M. (2010). Formation of the Late Permian Panzhihua Plutonic-Hypabyssal-Volcanic Igneous Complex: Implications for the Genesis of Fe-Ti Oxide Deposits and A-type Granites of SW China. *Earth Planet. Sci. Lett.* 289, 509–519. doi:10.1016/j.epsl.2009.11.044

Si, W., Hou, D., Wu, P., Zhao, Z., Ma, X., Zhou, H., et al. (2020). Geochemical Characteristics of Lower Cretaceous Lacustrine Organic Matter in the Southern Sag of the Wuliyasitai Depression, Erlian Basin, China. *Mar. Pet. Geology.* 118, 104404. doi:10.1016/j.marpetgeo.2020.104404

Su, C., Li, F., Tan, X., Gong, Q., Zeng, K., Tang, H., et al. (2020). Recognition of Diagenetic Contribution to the Formation of limestone-marl Alternations: A Case Study from Permian of South China. *Mar. Pet. Geology.* 111, 765–785. doi:10.1016/j.marpetgeo.2019.08.033

Tao, H., Qiu, Z., Lu, B., Liu, Y., and Qiu, J. (2020). Volcanic Activities Triggered the First Global Cooling Event in the Phanerozoic. *J. Asian Earth Sci.* 194, 104074. doi:10.1016/j.jseaes.2019.104074

Taylor, S. R., and McLennan, S. M. (1986). The Chemical Composition of the Archaean Crust. *Geol. Soc. Lond. Spec. Publications* 24, 173–178. doi:10.1144/GSL.SP.1986.024.01.16

Tuttle, M., Goldhaber, M., and Williamson, D. (1986). An Analytical Scheme for Determining Forms of sulphur in Oil Shales and Associated Rocks. *Talanta* 33, 953–961. doi:10.1016/0039-9140(86)80234-X

Uematsu, M., Toratani, M., Kajino, M., Narita, Y., Senga, Y., and Kimoto, T. (2004). Enhancement of Primary Productivity in the Western North Pacific Caused by the Eruption of the Miyake-Jima Volcano. *Geophys. Res. Lett.* 31, a–n. doi:10.1029/2003GL018790

Walker, L. R., Sikes, D. S., Degange, A. R., Jewett, S. C., Michaelson, G., Talbot, S. L., et al. (2013). Biological Legacies: Direct Early Ecosystem Recovery and Food Web Reorganization after a Volcanic Eruption in Alaska. *Écoscience* 20, 240–251. doi:10.2980/20-3-3603

Wang, C., Wang, Q., Chen, G., and Chen, D. (2021). Influence of Volcanism on the Development of Black Shales in the Chang 7 Member of Yanchang Formation in the Ordos Basin. *Int. J. Earth Sci. (Geol Rundsch)* 110, 1939–1960. doi:10.1007/s00531-021-02050-8

Wei, G. J., Li, X. H., Chen, Y. W., Liu, Y., and Chen, M. H. (2001). High-resolution Records of Transitive Metals of Sediments from Core NS93-5 and Their Paleoceanography Implications. *Geochimica* 5, 450–458.

White, J. D. L., and Houghton, B. F. (2006). Primary Volcaniclastic Rocks. *Geol* 34, 677–680. doi:10.1130/G22346.1

Winchester, J. A., and Floyd, P. A. (1977). Geochemical Discrimination of Different Magma Series and Their Differentiation Products Using Immobile Elements. *Chem. Geology.* 20, 325–343. doi:10.1016/0009-2541(77)90057-2

Witham, C. S., Oppenheimer, C., and Horwell, C. J. (2005). Volcanic Ash-Leachates: a Review and Recommendations for Sampling Methods. *J. Volcanology Geothermal Res.* 141, 299–326. doi:10.1016/j.jvolgeores.2004.11.010

Xiao, L., Xu, Y.-G., Chung, S.-L., He, B., and Mei, H. (2003). Chemostratigraphic Correlation of Upper Permian Lavas from Yunnan Province, China: Extent of the Emeishan Large Igneous Province. *Int. Geology. Rev.* 45, 753–766. doi:10.2747/0020-6814.45.8.753

Xiao, L., Xu, Y. G., Mei, H. J., Zheng, Y. F., He, B., and Pirajno, F. (2004). Distinct Mantle Sources of Low-Ti and High-Ti Basalts from the Western Emeishan Large Igneous Province, SW China: Implications for Plume-Lithosphere Interaction. *Earth Planet. Sci. Lett.* 228, 525–546. doi:10.1016/j.epsl.2004.10.002

Xu, Y., Chung, S.-L., Jahn, B.-m., and Wu, G. (2001). Petrologic and Geochemical Constraints on the Petrogenesis of Permian-Triassic Emeishan Flood Basalts in Southwestern China. *Lithos* 58, 145–168. doi:10.1016/S0024-4937(01)00055-X

Xu, Q., Fan, X.-M., Huang, R.-Q., and Westen, C. V. (2009). Landslide Dams Triggered by the Wenchuan Earthquake, Sichuan Province, South West China. *Bull. Eng. Geol. Environ.* 68, 373–386. doi:10.1007/s10064-009-0199-910.1007/s10064-009-0214-1

Xu, Y.-G., Chung, S.-L., Shao, H., and He, B. (2010). Silicic Magmas from the Emeishan Large Igneous Province, Southwest China: Petrogenesis and Their Link with the End-Guadalupian Biological Crisis. *Lithos* 119, 47–60. doi:10.1016/j.lithos.2010.04.013

Yan, C., Jin, Z., Zhao, J., Du, W., and Liu, Q. (2018). Influence of Sedimentary Environment on Organic Matter Enrichment in Shale: A Case Study of the Wufeng and Longmaxi Formations of the Sichuan Basin, China. *Mar. Pet. Geology.* 92, 880–894. doi:10.1016/j.marpetgeo.2018.01.024

Zeng, Z., Pike, M., Tice, M. M., Kelly, C., Marcantonio, F., Xu, G., et al. (2018). Iron Fertilization of Primary Productivity by Volcanic Ash in the Late Cretaceous (Cenomanian) Western Interior Seaway. *Geology* 46, 859–862. doi:10.1130/G45304.1

Zhang, K., Liu, R., Liu, Z., Li, B., Han, J., and Zhao, K. (2020). Influence of Volcanic and Hydrothermal Activity on Organic Matter Enrichment in the Upper Triassic Yanchang Formation, Southern Ordos Basin, Central China. *Mar. Pet. Geology.* 112, 104059. doi:10.1016/j.marpetgeo.2019.104059

Zhao, K., Du, X., Lu, Y., Hao, F., Liu, Z., and Jia, J. (2020). Is Volcanic Ash Responsible for the Enrichment of Organic Carbon in Shales? Quantitative Characterization of Organic-Rich Shale at the Ordovician-Silurian Transition. *GSA Bull.* 133, 837–848. doi:10.1130/B35737.1

Zhou, Y., Bohor, B. F., and Ren, Y. (2000). Trace Element Geochemistry of Altered Volcanic Ash Layers (Tonsteins) in Late Permian Coal-Bearing Formations of Eastern Yunnan and Western Guizhou Provinces, China. *Int. J. Coal Geology.* 44, 305–324. doi:10.1016/S0166-5162(00)00017-3

Zielinski, R. A. (1985). Element Mobility during Alteration of Silicic Ash to Kaolinite-A Study of Tonstein. *Sedimentology* 32, 567–579. doi:10.1111/j.1365-3091.1985.tb00471.x

Conflict of Interest: The authors declare that the research was conducted in the absence of any commercial or financial relationships that could be construed as a potential conflict of interest.

Publisher's Note: All claims expressed in this article are solely those of the authors and do not necessarily represent those of their affiliated organizations, or those of the publisher, the editors and the reviewers. Any product that may be evaluated in this article, or claim that may be made by its manufacturer, is not guaranteed or endorsed by the publisher.